Geochemical Perspectives Letters

© 2019 The Authors
Published by the European Association of Geochemistry

A lunar hygrometer based on plagioclase-melt partitioning of water

Y.H. Lin[1]*, H. Hui[2,3]*, Y. Li[4], Y. Xu[2], W. van Westrenen[1]*

OPEN ACCESS
doi: 10.7185/geochemlet.1908

Abstract

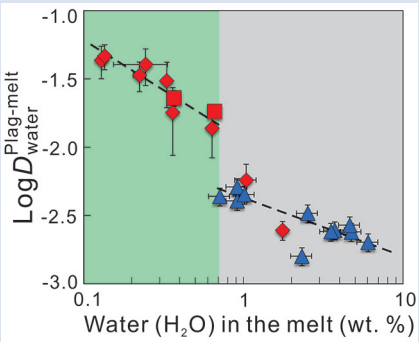

The Moon was initially covered by a magma ocean. Hydrogen detected in plagioclase of ferroan anorthosites, the only available samples directly crystallised from the lunar magma ocean (LMO), can be used to quantify LMO hydrogen content. We performed experiments to determine plagioclase-melt partition coefficients of water under LMO conditions with water contents of co-existing plagioclase and melt quantified using Fourier-Transform Infrared Spectroscopy. Results indicate lunar plagioclase can incorporate approximately one order of magnitude more water than previously assumed. Using measured water contents of lunar plagioclase, this suggests that ~100 μg/g H_2O equivalent was present in the residual magma when 95 % of the initial LMO had crystallised. Our results constrain initial LMO water contents to ~ 5 μg/g H_2O equivalent if water was conserved throughout LMO evolution. If on the other hand the initial LMO contained >1000 μg/g water as suggested by experiments on LMO crystallisation, >99 % hydrogen degassing occurred during the evolution of the LMO.

Received 5 December 2018 | Accepted 25 February 2019 | Published 26 March 2019

Introduction

The canonical view of a dry lunar interior has been challenged by detections of hydrogen (H or OH, reported here as equivalent amounts of H_2O in μg/g) in picritic glass beads (Saal *et al.*, 2008), apatites (*e.g.*, McCubbin *et al.*, 2010; Lin and van Westrenen, 2019), olivine-hosted melt inclusions (*e.g.*, Hauri *et al.*, 2011) and plagioclases (Hui *et al.*, 2013). Sample-based inferences about water in the Moon have been complemented by experimental and modelling studies of lunar magma ocean (LMO) crystallisation (Elkins-Tanton and Grove, 2011; Lin *et al.*, 2017a,b; Charlier *et al.*, 2018; Rapp and Draper, 2018). Quantification of the evolution of the lunar interior volatile budget would provide further insight into the thermal and magmatic evolution of the Moon. However, converting hydrogen abundance data measured in lunar samples or estimated from laboratory experiments to models of the temporal and spatial evolution of water in the Moon, is far from straightforward (McCubbin *et al.*, 2015a).

This study focuses on improving constraints on the water content in the Moon specifically during the LMO stage. Plagioclase is thought to have crystallised and floated to the surface during the late stages of LMO crystallisation, forming the lunar primary feldspathic crust (Warren, 1985). This indicates that plagioclase in lunar ferroan anorthosite could be our best candidate for estimating the water content of the LMO (Hui *et al.*, 2013, 2017). In addition, plagioclase could have formed continuously from ~70 % all the way up to >99 % of LMO crystallisation (Lin *et al.*, 2017a; Charlier *et al.*, 2018; Rapp and Draper, 2018). Therefore, the water content of plagioclase formed at different stages during LMO crystallisation could in principle be used to track and quantify the LMO water content through time.

While nominally anhydrous, terrestrial plagioclase can incorporate trace amounts of H as structural OH and/or molecular H_2O. In magmatic feldspars, concentrations from less than a few to more than 1000 μg/g H_2O have been reported (Johnson and Rossman, 2003, 2004; Johnson, 2006; Mosenfelder *et al.*, 2015). Only very few studies have measured water contents of lunar feldspars from a primary crystallisation product of the LMO so far (Hui *et al.*, 2013; 2017).

To link the water content in plagioclase to that in the melt from which the mineral crystallised, plagioclase-melt partition coefficients D of water are required, with $D^{plag\text{-}melt}_{water} = C^{plag}_{water} / C^{melt}_{water}$. Literature values for $D^{plag\text{-}melt}_{water}$ range between 0.002 ± 0.0004 and 0.006 ± 0.0009 (recalculated using the plagioclase absorption coefficient determined by Mosenfelder *et al.* (2015) based on measurements carried out

1. Faculty of Science, Vrije Universiteit Amsterdam, De Boelelaan 1085, 1081 HV Amsterdam, The Netherlands
2. State Key Laboratory for Mineral Deposits Research & Lunar and Planetary Science Institute, School of Earth Sciences and Engineering, Nanjing University, 163 Xianlin Dadao, Nanjing 210023, China
3. CAS Center for Excellence in Comparative Planetology, Hefei 230026, China
4. Guangzhou Institute of Geochemistry, Chinese Academy of Sciences, 511 Kehua Street, Tianhe District, Guangzhou 510640, China
* Corresponding authors (email: y.lin@vu.nl; hhui@nju.edu.cn; w.van.westrenen@vu.nl)

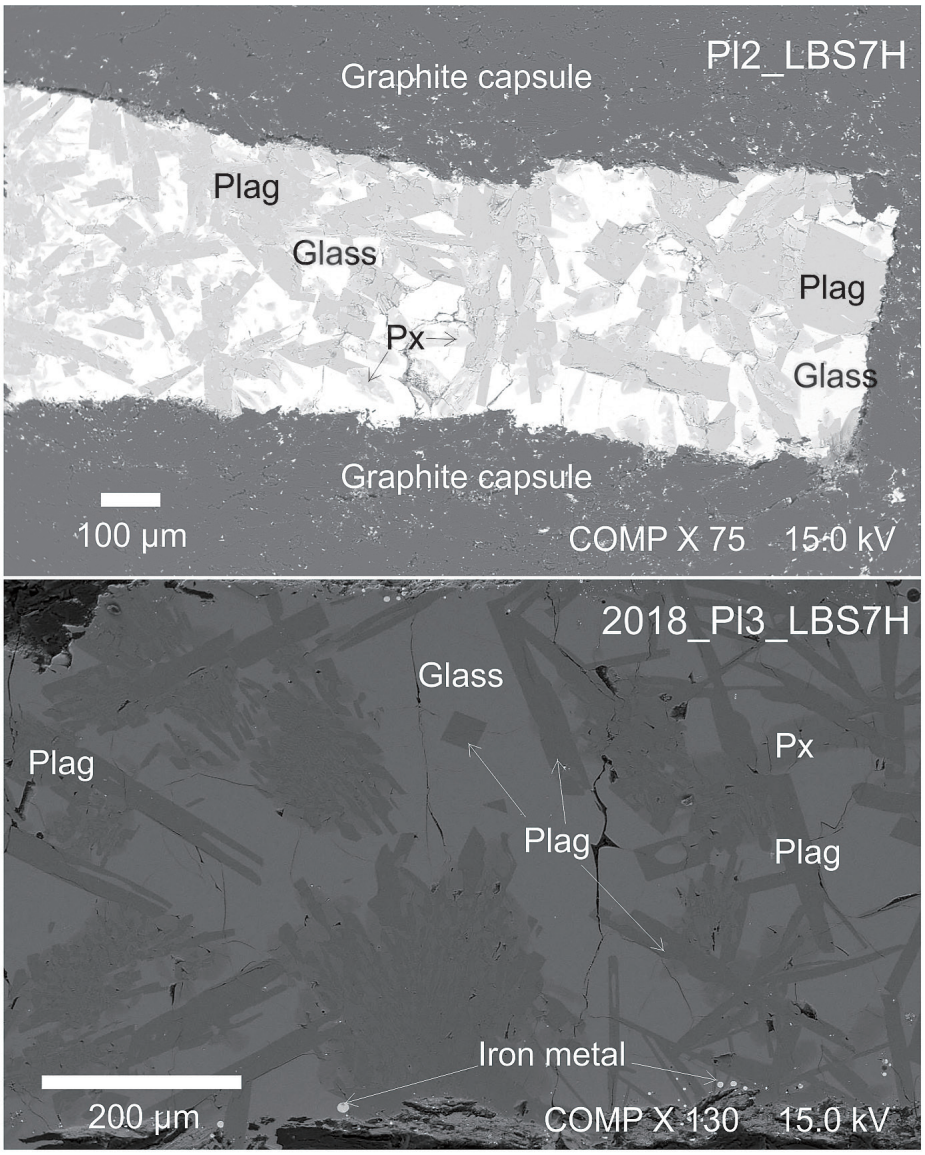

Figure 1 Backscattered electron (BSE) images of representative experimental run products (Pl2_LBS7H, 0.4 GPa – 1200 °C; and 2018_Pl3_LBS7H, 0.3 GPa – 1160 °C). Px = pyroxene; Plag = plagioclase.

in both natural and experimental systems, which have focused solely on magmatism on Earth (*e.g.*, Hamada *et al.*, 2013). To date, no plagioclase-melt partition coefficient of water under lunar conditions has been published. This is problematic, for example in terms of oxygen fugacity, as it has previously been suggested that fO_2 can affect hydrogen solubility in plagioclase (Yang, 2012). The available $D^{\text{plag-melt}}_{\text{water}}$ data, which are applied to terrestrial systems, were obtained at relatively oxidising conditions. The fO_2 in the Moon is thought to be significantly lower, at ~IW to ~IW-2 (IW: iron-wustite) (Sato *et al.*, 1973; Rutherford and Papale, 2009) based on sample analyses. In addition, although Yang (2012) suggests plagioclase composition, temperature and pressure have insignificant effects on $D^{\text{plag-melt}}_{\text{water}}$, this suggestion was based on experiments conducted in a limited temperature-pressure range.

In this study, $D^{\text{plag-melt}}_{\text{water}}$ was determined at pressure-temperature-composition conditions occurring in the lunar magma ocean using high pressure and high temperature experiments and Fourier-Transform Infrared Spectroscopy (FTIR). The pressures (0.4–0.6 GPa) and temperatures (1130–1220 °C) were chosen to be consistent with plagioclase formation during crystallisation of a water-bearing lunar magma ocean (Lin *et al.*, 2017a). The main purposes of this paper are: (1) to quantify the effects of composition and fO_2 on $D^{\text{plag-melt}}_{\text{water}}$, and (2) to offer further constraints on the water content of the LMO at the time of plagioclase crystallisation.

Water Partition Coefficients

Details of high pressure, high temperature, plagioclase-melt partitioning experiments are given in the Supplementary Information. Table 1 provides a summary of experimental *P-T-fO*$_2$ conditions. Starting compositions, EMPA analyses of the major element concentrations in plagioclase and melt phases in the experimental run products, and log(fO_2) calculations are shown in Tables S-1 and S-2 of the Supplementary Information. All experimental charges contain plagioclase, pyroxene, and quenched glass (Fig. 1). One experimental charge contains Fe metal in addition, indicating an oxygen fugacity at or below that of the iron-wüstite buffer. Representative unpolarised FTIR spectra of plagioclase are shown in Figure 2. All plagioclases show absorption bands (~3000–3600 cm^{-1}) in the mid-infrared region typical of O–H bonds (Johnson and Rossman, 2004). No H_2 bands have been observed in our plagioclase spectra. Further descriptions are shown in the Supplementary Information.

Table 1 gives FTIR-derived H_2O concentrations in plagioclase and glass from our work, Hamada *et al.* (2013) and Caseres *et al.* (2017). The H_2O equivalent concentrations in our samples range from 42 ± 6 to 99 ± 36 μg/g in plagioclase and 0.13 ± 0.01 to 1.74 ± 0.01 wt. % in silicate glass. The corresponding partition coefficients range between 0.0020 ± 0.0004 and 0.0460 ± 0.0096.

The H_2O concentrations in our plagioclase crystals are significantly below water solubility at our experimental conditions (Yang, 2012). Sample 2018_Pl17_LBS8H, with glass containing the highest water concentration (1.74 wt. % H_2O), has the lowest water concentration in plagioclase (42 μg/g H_2O) and hence the lowest partition coefficient ($D^{plag\text{-}melt}_{water}$ = 0.0020 ± 0.0004). This lowest value is at the lower end of the range of previously published partition coefficients ($D^{plag\text{-}melt}_{water}$ = 0.002–0.006) by Hamada *et al.* (2013). Our highest partition coefficient is ~7–20 times higher than values from the Hamada *et al.* (2013) data set. The water partition coefficients reported by Caseres *et al.* (2017; $D^{plag\text{-}melt}_{water}$ = 0.018–0.023 at the IW buffer) overlap with our results.

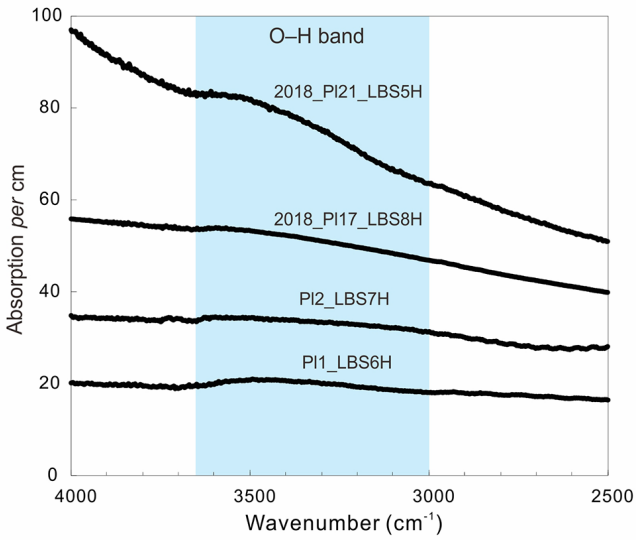

Figure 2 Representative unpolarised infrared spectra of plagioclase, normalised to 1 cm thickness. Spectra are shifted vertically to facilitate comparison.

Table 1 Summary of experimental conditions and water contents of run products in our experiments and literature data.

Sample	Conditions			Plagioclase			Glass			Water partition coefficient		Oxygen fugacity	
	P (GPa)	T °C	Duration (h)	OH (μg/g H_2O)	n	1 s.d.	OH (wt.% H_2O)	n	1 s.d.	$D^{plag\text{-}melt}$	1 s.d.	Oxygen buffer	Log (fO_2)
This study													
Pl1_LBS6H	0.4	1160	14	58.2	11	17.9	1.03	9	0.16	0.006	0.002		-10.4
Pl2_LBS7H		1200	16	63.2	9	32.8	0.35	10	0.02	0.018	0.009		-10.0
Pl3_LBS8H_1		1160	22	96.0	4	28.8	0.24	12	0.09	0.040	0.012		-10.4
Pl4_LBS8H_2		1180	14	85.5	5	33.8	0.63	8	0.04	0.014	0.005	Graphite–COH (C–COH)	-10.2
Pl5_LBS8H_3		1180	18	99.1	6	36.4	0.32	10	0.01	0.030	0.011		-10.2
2018_Pl2_LBS8H		1170	24	73.4	7	17.0	0.22	8	0.02	0.034	0.008		-10.3
2018_Pl17_LBS8H		1180	24	42.2	8	6.64	1.74	9	0.01	0.002	0.000		-10.2
2018_Pl21_LBS5H		1190	24	54.2	6	14.2	0.13	8	0.01	0.043	0.012		-10.1
2018_Pl3_LBS7H	0.3	1160	24	61.1	7	12.602	0.13	11	0.004	0.046	0.010	Iron-Wustite (IW)	-12.4
Caseres *et al.* (2017)													
1#	0.8	1150		82		11	0.36		0.003	0.023	0.003	Iron-Wustite (IW)	-12.3
2#				118		6	0.65		0.008	0.018	0.001		-12.3
Hamada *et al.* (2013)													
MTL04	0.35	1130	24	89.8		13.5	3.70		0.56	0.002	0.000		
MTL05		1170	24	80.8		12.1	2.50		0.38	0.003	0.000		
MTL17		1220	24	35.9		5.4	0.90		0.14	0.004	0.001		
MTL22		1130	24	36.0		5.4	2.30		0.35	0.002	0.000		-4.7
MTL26		1160	24	30.1		4.5	0.70		0.11	0.004	0.001		
MTL29		1170	24	45.4		6.8	0.90		0.14	0.005	0.001	> Ni–NiO (NNO)	-5.2
MTL33		1230	24	44.4		6.7	1.00		0.15	0.004	0.001		-5.8
MTL37		1070	24	111		16.6	4.70		0.71	0.002	0.000		-5.2
MTL39		1100	24	82.9		12.4	3.50		0.53	0.002	0.000		
MTL40		1100	24	121		18.2	4.60		0.69	0.003	0.000		-4.7
MTL41		1050	24	119		17.8	6.00		0.90	0.002	0.000		
Melt Inclusion													
Pl19-MI				15.3		2.3	0.32		0.05	0.005	0.001		
Pl21-MI				10.6		1.6	0.24		0.04	0.004	0.001	Fe_2SiO_4–Fe_3O_4–SiO_2 (FMQ)	
Pl22-MI				16.4		2.5	0.26		0.04	0.006	0.001		

Note: n, number of analysed plagioclases; s.d., 1 sigma standard deviation; Log fO_2(buffer) corrected in the Supplementary Information;
Melt inclusion data not used in this study because we do not know exact T, P, and whether there was any water loss from the inclusions after formation;
The latest infrared absorption coefficient (Mosenfelder *et al.*, 2015) was used for calibrating water contents of all plagioclases.

The Effects of Oxygen Fugacity and Water Content in Melt

It has been shown that a number of parameters can affect water partitioning between nominally anhydrous minerals and silicate melts, including the presence and abundance of chemical impurities and vacancies, the possibility of substitutions with charge-balancing species, temperature, pressure, and oxygen fugacity (*e.g.*, Yang, 2012 and references therein). Previous work on water solubility in feldspar has shown that there is no obvious compositional dependence on the incorporation of H in the feldspar group except for a possible link with potassium content or sodium-hydrogen diffusion during heating (Yang, 2012; Johnson and Rossman, 2013). Potassium, however, has very low concentrations in ferroan anorthositic plagioclase, <0.03 wt. % (Dixon and Papike, 1975) and is absent in our experiments. Pressure and temperature effects cannot be assessed on the basis of our experiments, and those of Hamada *et al.* (2013) and Caseres *et al.* (2017), due to the overall limited pressure (0.3–0.8 GPa) and temperature (1000–1230 °C) range.

The H solubility in Fe-poor plagioclase near the IW buffer was demonstrated to be more than twice that determined at more oxidising conditions (Yang, 2012), leading to the hypothesis that oxygen fugacity could cause the difference between data obtained at lunar conditions, including our data and the data of Caseres *et al.* (2017), and those obtained at terrestrial conditions, *i.e.* the data of Hamada *et al.* (2013). However, Figure 3a shows that there is no correlation between $D^{\text{plag-melt}}_{\text{water}}$ and fO_2 in the overall data set. The terrestrial data set at relatively oxidising conditions yields lower $D^{\text{plag-melt}}_{\text{water}}$ than the lunar data sets obtained at lower fO_2, similar to the trend between oxygen fugacity and hydrogen solubility in plagioclase (Yang, 2012). One possibility is that the number of vacancies available for hydrogen incorporation is increased at low fO_2, for example due to the enhanced incorporation of divalent iron in Al sites (Mosenfelder *et al.*, 2019). However, although high values are found at low fO_2, some low-fO_2 experiments show low $D^{\text{plag-melt}}_{\text{water}}$ (Fig. 3a). Oxygen fugacity is therefore not the main factor affecting $D^{\text{plag-melt}}_{\text{water}}$. Instead, the experiments suggest that the water content of the silicate melt plays a key role in determining the partition coefficient of water between plagioclase and melt (Fig. 3b). There is an inverse relationship between the measured $D^{\text{plag-melt}}_{\text{water}}$ and the water concentration in silicate melt. In the absence of a theoretical framework to guide the functional form used to describe these inverse relations, we provide the following best-fit equations:

$$D^{\text{plag-melt}}_{\text{water}} = -6\cdot10^{-2}\cdot x + 0.05 \ (x \leq 0.7;\ R^2 = 0.85), \quad \text{Eq. 1a}$$

$$D^{\text{plag-melt}}_{\text{water}} = -5\cdot10^{-4}\cdot x + 0.005 \ (x > 0.7;\ R^2 = 0.60), \quad \text{Eq. 1b}$$

where x is wt. % H_2O in the silicate melt. Equations 1a and 1b provide quantitative estimates of $D^{\text{plag-melt}}_{\text{water}}$ given ranges of the magma oxygen fugacity and water content in silicate melt.

The exact mechanism controlling the observed variations of $D^{\text{plag-melt}}_{\text{water}}$ with fO_2 and water content cannot be derived from our experiments, and it is not feasible to construct a thermodynamics-based predictive model of $D^{\text{plag-melt}}_{\text{water}}$ with the currently available data sets. Clearly water partitioning shows strong non-Henrian behaviour in our experiments, pointing to non-ideal behaviour of the relevant hydrogen-bearing species in mineral and/or melt. Previous work has suggested that changes in the OH site in plagioclases occur as a function of plagioclase OH content (Hamada *et al.*, 2013), but we cannot identify variations in the shape of the FTIR spectra that would be consistent with such a change in our experiments. It therefore seems more likely that the non-Henrian behaviour is caused by water activity coefficient changes in the melt. The dominant hydrogen-bearing species in hydrous melts at the hydrogen levels in our experiments could be OH (Stolper, 1982; Newcombe *et al.*, 2017), but non-linear increases in the H_2O/OH ratio with increasing silicate melt hydrogen content have previously been observed (Stolper, 1982). These speciation changes affect the OH activity in the silicate melts, consistent with the observed trend in $D^{\text{plag-melt}}_{\text{water}}$ values, though future work is needed to quantify this correlation.

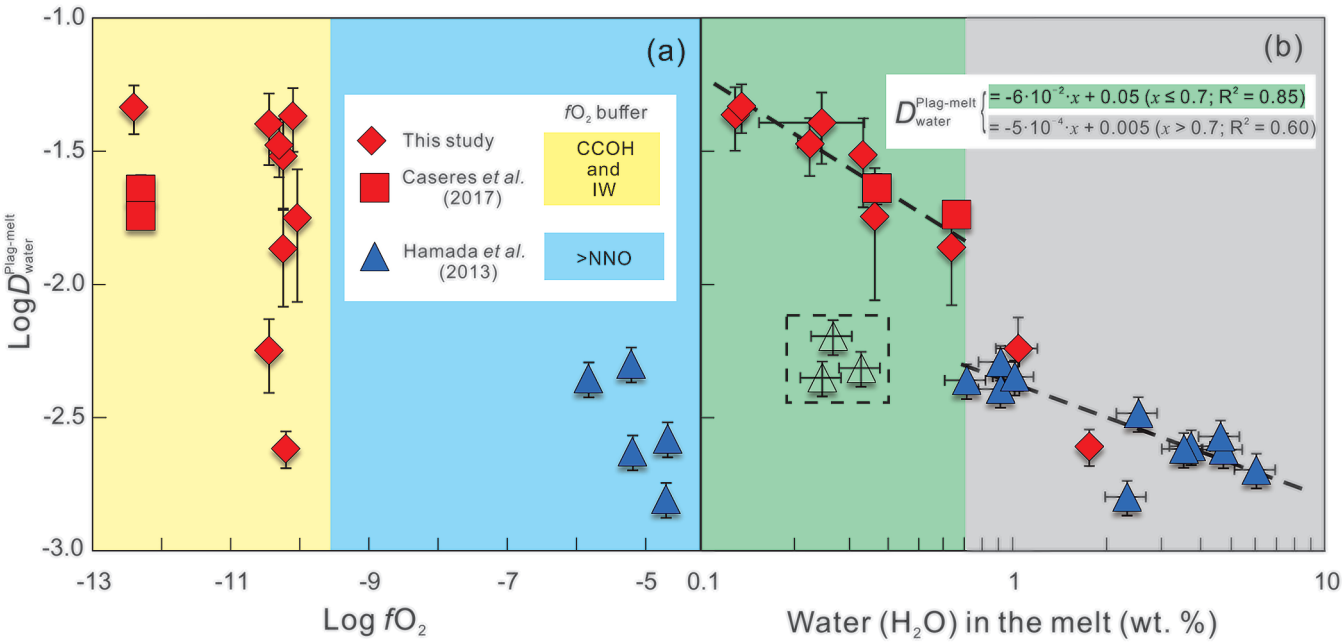

Figure 3 Partition coefficients of water between plagioclase and melt from this study and literature data (Hamada *et al.*, 2013; Caseres *et al.*, 2017), plotted *versus* **(a)** oxygen fugacity, and **(b)** water concentration in silicate melt. Melt inclusion data (Hamada *et al.*, 2013) in the dotted box are not used in this study because the formation temperature of these inclusions and the degree of water loss from inclusions after formation are uncertain.

Water Content of the Lunar Magma Ocean

Equation 1a can be used to calculate the water content of the LMO at lunar oxygen fugacity conditions. This calculation requires estimates of (a) the abundance of water in lunar plagioclase, and (b) the degree of crystallisation of the LMO at the time of plagioclase formation.

The latest study published to date on the water content of lunar plagioclase from a primary crystallisation product of the LMO reported ~5 μg/g water (H_2O) in ferroan anorthosite samples including Apollo sample 60015 (Hui *et al.*, 2017). We constrained the degree of crystallisation of the LMO when this plagioclase was formed by comparing the Mg# (molar (MgO/MgO + FeO) × 100) of plagioclase from sample 60015 (Mg# of 17–47) (Dixon and Papike, 1975) to the Mg# of plagioclase formed at different stages from our recent experimental study of LMO crystallisation (Lin *et al.*, 2017a,b). The first plagioclase formed during LMO crystallisation has a Mg# of ~60. This Mg# decreases with progressive crystallisation. Plagioclase with Mg# as low as 17–47 forms after ~95 % crystallisation of the LMO.

Based on the above constraints, the amount of H_2O equivalent in the residual LMO after ~95 % solidification of the initial magma ocean is calculated to be ~100 μg/g by solving the equation $D^{\text{plag-melt}}_{\text{water}} = 5/C^{\text{melt}}_{\text{water}} = -6{\cdot}10^{-2}{\cdot}(C^{\text{melt}}_{\text{water}}/10000) + 0.05$ (here, $C^{\text{melt}}_{\text{water}}$ is in μg/g). If the LMO hydrogen budget remained constant throughout LMO solidification, this implies a very low initial LMO water content of just 5 μg/g H_2O equivalent, consistent with inferences from petrology and magma ocean modelling (Elkins-Tanton and Grove, 2011), lunar sample measurements (McCubbin *et al.*, 2015b), and the experimental LMO solidification studies of Rapp and Draper (2018) and Charlier *et al.* (2018). In contrast, if the *initial* LMO contained >500–1800 μg/g water as suggested by the experimental LMO solidification study of Lin *et al.* (2017a) the minimum amount of water in the *residual* LMO at the time of lunar plagioclase formation would have exceeded 1 wt. %, far exceeding the ~100 μg/g estimated using the plagioclase hygrometer in this study. In this case, the early Moon experienced extensive degassing, with >99 % of the initial LMO water budget lost during LMO crystallisation. Such a high degree of degassing is consistent with observations based on the isotopic compositions of hydrogen of lunar plagioclase (Hui *et al.*, 2017) and of chlorine in lunar apatites (Sharp *et al.*, 2010) if degassing of Cl occurred primarily through metal chlorides (*e.g.*, Schaefer and Fegley, 2004; Sarafian *et al.*, 2017), and would point to a highly dynamic volatile cycle during early lunar evolution.

Acknowledgements

We dedicate this manuscript to the memory of Erik Hauri. We thank Fei Peng and Wei Chen for technical assistance during electron microprobe analyses and experiments. Dr. Francis McCubbin and Dr. Adam Sarafian are thanked for their constructive reviews, and Dr. Horst R. Marschall is thanked for the editorial handling. This work was supported financially by a Netherlands Organization for Scientific Research (N.W.O.) Vici grant and N.W.O. User Support Programme Space Research grant to WvW, National Natural Science Foundation of China grants (41573055 and 41590623) to HH, Royal Netherlands Academy of Arts and Sciences China Exchange Programme grant (530-6CDP20) to WvW, HH, and YHL, National Natural Science Foundation of China grant (U1530402) to HKM, and partially supported by the Key Research Program of the Chinese Academy of Sciences, Grant NO. XDPB11, Strategic Priority Research Program (B) of the Chinese Academy of Sciences (XDB18020301) to YL, and Key Research Program of Frontier Sciences (QYZDJ-SSW-DQC012) of the CAS to XX.

Editor: Horst R. Marschall

Author Contributions

YHL, HH, and WvW. designed this project. YHL. performed the experiments. YJX, YHL, and HH performed the FTIR analyses. YHL wrote the paper with input from all co-authors.

Additional Information

Supplementary Information accompanies this letter at http://www.geochemicalperspectivesletters.org/article1908.

This work is distributed under the Creative Commons Attribution 4.0 License, which permits unrestricted use, distribution, and reproduction in any medium, provided the original author and source are credited. Additional information is available at http://www.geochemicalperspectivesletters.org/copyright-and-permissions.

Cite this letter as: Lin, Y.H., Hui, H., Li, Y., Xu, Y., van Westrenen, W. (2019) A lunar hygrometer based on plagioclase-melt partitioning of water. *Geochem. Persp. Let.* 10, 14–19.

References

Caseres, J.R., Mosenfelder, J.L., Hirschmann, M.M. (2017) Partitioning of hydrogen and fluorine between feldspar and melt under the conditions of lunar crust formation. *Lunar and Planetary Science Conference* 48, 2303.

Charlier, B., Grove, T.L., Namur, O., Holtz, F. (2018) Crystallization of the lunar magma ocean and the primordial mantle-crust differentiation of the Moon. *Geochimica et Cosmochimica Acta* 234, 50–69.

Dixon, J.R., Papike, J.J. (1975) Petrology of anorthosites from the Descartes region of the Moon: Apollo 16. *Lunar and Planetary Science Conference* 6, 263–291.

Elkins-Tanton, L.T., Grove, T.L. (2011) Water (hydrogen) in the lunar mantle: Results from petrology and magma ocean modeling. *Earth and Planetary Science Letters* 307, 173–179.

Hamada, M., Ushioda, M., Fujii, T., Takahashi, E. (2013) Hydrogen concentration in plagioclase as a hygrometer of arc basaltic melts: Approaches from melt inclusion analyses and hydrous melting experiments. *Earth and Planetary Science Letters* 365, 253–262.

Hauri, E.H., Weinreich, T., Saal, A.E., Rutherford, M.C., van Orman, J.A. (2011) High pre-eruptive water contents preserved in lunar melt inclusions. *Science* 213, 10–13.

Hui, H., Peslier, A.H., Zhang, Y., Neal, C.R. (2013) Water in lunar anorthosites and evidence for a wet early moon. *Nature Geoscience* 6, 177–180.

Hui H., Guan, Y., Chen, Y., Peslier, A.H., Zhang, Y., Liu, Y., Flemming, R.L., Rossman, G.R., Eiler, J.M., Neal, C.R., Osinski, G.R. (2017) A heterogeneous lunar interior for hydrogen isotopes as revealed by the lunar highlands samples. *Earth and Planetary Science Letters* 473, 14–23.

Johnson, E.A. (2006) Water in nominally anhydrous crustal minerals: speciation, concentration, and geologic significance. *Reviews in Mineralogy and Geochemistry* 62, 117–154.

Johnson, E.A., Rossman, G.R. (2003) The concentration and speciation of hydrogen in feldspars using FTIR and ^{1}H MAS NMR spectroscopy. *American Mineralogist* 88, 901–911.

Johnson, E.A., Rossman, G.R. (2004) A survey of hydrous species and concentrations in igneous feldspars. *American Mineralogist* 89, 586–600.

Johnson, E.A., Rossman, G.R. (2013) The diffusion behavior of hydrogen in plagioclase feldspar at 800-1000°C: Implications for re-equilibration of OH in volcanic phenocrysts. *American Mineralogist* 98, 1779–1787.

Lin, Y.H., Tronche, E.J., Steenstra, E.S., van Westrenen, W. (2017a) Evidence for an early wet Moon from experimental crystallization of the lunar magma ocean. *Nature Geoscience* 10, 14–18.

Lin, Y.H., Tronche, E.J., Steenstra, E.S., van Westrenen, W. (2017b) Experimental constraints on the solidification of a nominally dry lunar magma ocean. *Earth and Planetary Science Letters* 471, 104–116.

Lin, Y.H., van Westrenen, W. (2019) Isotopic evidence for volatile replenishment of the Moon during Late Accretion. *National Science Review,* doi: 10.1093/nsr/nwz033.

McCubbin, F.M., Steele, A., Hauri, E.H., Nekvasil, H., Yamashita, S., Hemley, R.J. (2010) Nominally hydrous magmatism on the Moon. *Proceedings of the National Academy of Sciences of the United States of America* 107, 11223–11228.

McCubbin, F.M., Vander Kaaden, K.E., Tartèse, R., Boyce, J.W., Mikhail, S., Whitson, E.S., Bell, A.S., Anand, M., Franchi, I.A., Wang, J., Hauri, E.H. (2015a) Experimental investigation of F, Cl, and OH partitioning between apatite and Fe-rich basaltic melt at 1.0–1.2 GPa and 950–1000 °C. *American Mineralogist* 100, 1790–1802.

McCubbin, F.M., Vander Kaaden, K.E., Tartèse, R., Klima, R.L., Liu, Y., Mortimer, J., Barnes, J., Shearer, C.K., Treiman, A.H., Lawrence, D.J., Elardo, S.M., Hurley, D.M., Boyce, J.W., Anand, M. (2015b) Magmatic volatiles (H, C, N, F, S, Cl) in the lunar mantle, crust, and regolith: Abundances, distributions, processes, and reservoirs. *American Mineralogist* 100, 1668–1707.

Mosenfelder, J.L., Rossman, G.R., Johnson, E.A. (2015) Hydrous species in feldspars: A reassessment based on FTIR and SIMS. *American Mineralogist* 100, 1209–1221.

Mosenfelder, J.L., Andrys, J.L., Caseres, J.R., Hirschmann, M.M. (2019) Water in the Moon: The perspective from nominally anhydrous minerals. *Lunar and Planetary Science Conference* 50, 2132.

Newcombe, M.E., Brett, A., Beckett, J.R., Baker, M.B., Newman, S., Guan, Y., Eiler, J.M., Stolper, E.M. (2017) Solubility of water in lunar basalt at low pH_2O. *Geochimica et Cosmochimica Acta* 200, 330–352.

Rapp, J.F., Draper, D.S. (2018) Fractional crystallization of the lunar magma ocean: Updating the dominant paradigm. *Meteoritics and Planetary Science* 53, 1432–1455.

Rutherford, M.J., Papale, P. (2009) Origin of basalt fire-fountain eruptions on Earth versus the Moon. *Geology* 37, 219–222.

Saal, A.E., Hauri, E.H., Cascio, M.L., Van Orman, J.A., Rutherford, M.C., Cooper, R.F. (2008) Volatile content of lunar volcanic glasses and the presence of water in the Moon's interior. *Nature* 454, 192–195.

Sarafian, A.R., John, T., Roszjar, J., Whitehouse, M.J. (2017) Chlorine and hydrogen degassing in Vesta's magma ocean. *Earth and Planetary Science Letters* 459, 311–319.

Sato, M., Hickling, N.L., McLane, J.E. (1973) Oxygen fugacity values of Apollo 12, 14, and 15 lunar samples and reduced state of lunar magmas. *Proceedings of the Lunar Science Conference* 1, 1061–1079.

Schaefer, L., Fegley, B. (2004) A thermodynamic model of high temperature lava vaporization on Io. *Icarus* 169, 216–241.

Sharp, Z.D., Shearer, C.K., McKeegan, K.D., Barnes, J.D., Wang, Y.Q. (2010) The chlorine isotope composition of the Moon and implications for an anhydrous mantle. *Science* 329, 1050–1053.

Stolper, E. (1982) Water in silicate glasses: An infrared spectroscopic study. *Contributions to Mineralogy and Petrology* 81, 1–17.

Warren, P.H. (1985) The magma ocean concept and lunar evolution. *Annual Review of Earth and Planetary Sciences* 13, 201–240.

Yang, X. (2012) An experimental study of H solubility in feldspars: Effect of composition, oxygen fugacity, temperature and pressure and implications for crustal processes. *Geochimica et Cosmochimica Acta* 97, 46–57.

Geochemical Perspectives Letters

© 2019 The Authors
Published by the European Association of Geochemistry

A lunar hygrometer based on plagioclase-melt partitioning of water

Y.H. Lin, H. Hui, Y. Li, Y. Xu, W. van Westrenen

Supplementary Information

The Supplementary Information includes:

- 1. Experimental and Analytical Methods
- 2. Accuracy of Partition Coefficients
- 3. Oxygen Fugacity Calculations
- Tables S-1 and S-2
- Figures S-1 and S-2
- Supplementary Information References

1. Experimental and Analytical Methods

Starting Materials

The compositions of our starting materials and the experimental pressure-temperature conditions were based on an experimental study of LMO crystallisation, which has shown that plagioclase starts to crystallise after approximately 75% solidification of a bulk silicate Earth-like lunar magma ocean in water-bearing experiments (Lin *et al*., 2017a). The water-bearing bulk compositions that yielded plagioclase (steps LBS6H, LBS7H, and LBS8H from Lin *et al*. (2017a)) were chosen as starting compositions for our partitioning study. Starting materials were prepared by mixing appropriate amounts of high purity (99.5–99.99 %, Alfa Aesar) powdered (hydr)oxides (MgO, $Mg(OH)_2$, Fe_2O_3, Al_2O_3, $Al(OH)_3$, TiO_2, SiO_2) and $CaCO_3$ (99.95–100.05 %, Alfa Aesar). The oxides MgO, Al_2O_3, TiO_2 and SiO_2 were first fired overnight at 1000 °C and then stored at 110 °C until use. The other oxides, hydroxides and calcium carbonate were dried at 110 °C overnight prior to use. The nominally dry starting chemicals were mixed in ethanol using an agate mortar for 1 hour, and then the mixtures were dried in air and decarbonated in a Pt crucible in a box furnace by gradually raising the temperature from 650 to 1000 °C in approximately 7 hours. The Pt crucible had previously been iron-saturated to minimise iron loss. The mixtures were melted by heating to 1550 °C. The melts were kept at this high temperature for 20 minutes to promote homogeneity, and to reduce most of the iron in the starting material to Fe^{2+}. The melts were quenched to glass by immersing the bottom of the Pt crucible in water. The glass samples were subsequently crushed, dried, and ground in ethanol using an agate mortar for 1 hour and then kept at 110 °C until use. Water was added to nominally dry glass using $Mg(OH)_2$. The starting material compositions for water partitioning experiments, containing between 0.53 and 0.87 wt. % H_2O, are presented in Table S-1.

High-pressure Experiments

High-pressure, high-temperature partitioning experiments were performed in a piston cylinder press using a half-inch (12.7 mm) diameter talc-pyrex cell assembly (van Kan Parker *et al.*, 2011). For these experiments, a hand-machined graphite bucket with an inner diameter (ID) of 0.7 mm, outer diameter (OD) of ~1.7 mm, and a length of 3–4 mm, was filled with starting material, closed with a graphite lid and inserted in a gold-palladium ($Au_{80}Pd_{20}$) capsule, with an ID of 1.7 mm, OD of 2 mm, and a length of 5–7 mm. The bottom end of the $Au_{80}Pd_{20}$ capsule was triple crimped, flattened and welded shut. After the graphite capsule was inserted, the other end of the $Au_{80}Pd_{20}$ capsule was crimped and welded shut. The use of a graphite inner capsule ensures that the oxygen fugacities of these experiments are significantly lower than in previous studies focused on terrestrial conditions (Ulmer and Luth, 1991; see section 3 below). Temperatures were monitored using a W_5Re–$W_{26}Re$ (type C) thermocouple and Omega® CN76000 programmable controller. The sample center was located at the hotspot of the assembly, 2 mm away from the thermocouple tip end, so that the sample temperatures were within 10 °C of the thermocouple reading (Watson *et al.*, 2002). Experiments were pressurised cold and then heated to a superliquidus temperature of 1280 °C for 20 minutes. Subsequently, samples were cooled to the temperature of interest at a rate of 10 °C per hour while maintaining target pressure, and kept for 14–24 hours at target temperature. Target pressures were 0.3 or 0.4 GPa for all experiments conducted in this study, and final target temperatures ranged from 1160 to 1200 °C. At completion of each experiment, the sample assembly was quenched by cutting power to the heater and the temperature dropped below the glass transition temperature in <10 s.

Analytical Techniques and Procedures

Experimental run products were mounted in epoxy and polished into thick sections. The sections were carbon coated for back-scattered electron (BSE) imagery to assess texture and mineralogy and subsequent electron microprobe analysis (EMPA). The chemical compositions of the run product phases (minerals and quenched glasses) were determined using a JEOL JXA-8800M Electron Microprobe at Guangzhou Institute of Geochemistry, Chinese Academy of Sciences calibrated with primary standards of diopside (Ca, Si), fayalite (Fe), ilmenite (Ti), olivine (Mg) and orthoclase (Al). Analyses were carried out using an accelerating voltage of 15 kV and a beam current of 20 nA. Focused beams with 1 and 10 μm diameter were used for the mineral phases and quenched glasses, respectively. Peak count times were 20 seconds and background count times were 10 seconds. Compositions reported here are based on the average of 5–10 analyses. The modal abundances of all mineral and glass phases were determined using mass balance calculations, which agree well with the estimates derived from phase area percentages obtained using an EDAX-EDS system in imaging mode.

After EMPA analyses, carbon coatings were removed and experimental samples were doubly polished into sections with thicknesses ranging from 50 to 180 μm (measured with Mitutoyo thickness gauge) using abrasive paper and aluminum oxide powder. Subsequently, doubly-polished samples were successively cleaned using acetone, ethanol and deionised water in an ultrasonic cleaner, and then dried in air at room temperature. Finally, the dried sample sections were stored in a desiccator for 24 hours to eliminate potential water adsorbed on the surface of sample sections.

Water concentrations in minerals and coexisting glass in our samples were obtained at the State Key Laboratory for Mineral Deposits Research, Nanjing University, using a Continuμm microscope attached to a Nicolet IS50 Fourier transform infrared (FTIR) spectrometer. A liquid nitrogen cooled MCT/A detector and KBr beam splitter were used during FTIR analyses. The infrared light pathway was flushed with dried N_2 to minimise interference from atmospheric water vapor. Spectra (wavenumbers from 700 to 7000 cm^{-1}) with a resolution of 4 cm^{-1} were collected after 1024 scans for each FTIR analysis. Aperture sizes ranging from 50×50 μm to 15×15 μm were chosen on the basis of the dimensions of crystals and glass. Visible cracks were avoided to minimise possible contamination during FTIR measurements.

Water concentrations in analysed crystals and glass were calculated using the following equation according to the Beer-Lambert law:

$$c\ (\mathrm{wt.\%}) = \frac{1.802 \cdot A_{\mathrm{tot}}}{\rho \cdot t \cdot \varepsilon} \qquad \text{Eq. S-1}$$

where c is the water concentration of the mineral (wt. %), A_{tot} is the integral area under the absorption bands of interest on infrared spectra (cm^{-1}), ρ is the mineral density ($g \cdot cm^{-3}$), t is the sample thickness (cm), and ε is the integral molar absorption coefficient ($l \cdot mol^{-1} \cdot cm^{-2}$). Quantification of water concentrations in an anisotropic mineral normally requires analyses of oriented crystals using polarized light along the three principal optical directions. However, due to the difficulty of obtaining oriented plagioclase grains from the experimental charges, it was not possible to make measurements with a polarised infrared beam along the three principal axes of crystals. Therefore, the method using unpolarized infrared spectra of randomly oriented crystals (Kovács *et al.*, 2008; Sambridge *et al.*, 2008) was used to determine the water contents of our crystals. We have used the recently published water

absorption coefficient for Ca-rich plagioclase of 202600 ± 20260 l mol^{-1} cm^{-2} (Mosenfelder *et al.*, 2015) to convert infrared intensities to water contents in our anorthitic plagioclase crystals, and to enable comparison with previous work recalculated the previously published water concentrations of Ca-rich plagioclases from Hamada *et al.* (2013), in which an older estimate of the absorption coefficient of 107000 ± 5000 l mol^{-1} cm^{-2} (Johnson and Rossman, 2003) was used. A density of 2760 kg m^{-3} was used for plagioclase in Equation S-1.

To calculate water concentrations in silicate glass, the total absorbance A_{tot} is replaced by the peak height of the band at wavenumber ~3550 cm^{-1} on the unpolarised infrared spectra, and ρ is the density of basaltic glass (2819 kg·m^{-3} used in this study following Yamashita *et al.* (1997) and Hamada *et al.* (2013)). The molar absorption coefficient of 64 ± 1 l·mol^{-1}·cm^{-1} (Yamashita *et al.*, 1997) was used for basaltic glass.

2. Accuracy of Partition Coefficients

Plagioclase and glass compositions are very similar to those reported in Lin *et al.* (2017a) in terms of major and minor elements. In the absence of sodium and potassium, plagioclases are near-pure anorthite containing minor amounts of titanium, iron, and magnesium (Table S-2), and there is no obvious relationship between these elements and water content in our data. Glasses contain 45 ~ 49 wt. % SiO_2, typical for lunar magma ocean melts in equilibrium with plagioclase (Lin *et al.*, 2017a). Lengths and widths of the cross-sections of analysed plagioclase crystals range from 100 to 300 μm and from 50 to 150 μm, respectively (Fig. 1).

The plagioclase FTIR spectra in Fig. 2 are very similar to published spectra of natural plagioclase grains containing OH (Yang *et al.*, 2015; Liu *et al.*, 2018), in particular spectra of grains that were heated to high temperatures. The water absorption peaks in all glass samples are also centered at a wavenumber of ~3570 cm^{-1}. Furthermore, the H_2 bands, shown in the spectra of Yang *et al.* (2016), were not observed in our plagioclase spectra.

Because the water abundances in nominally anhydrous plagioclase are low, we performed multiple tests to confirm the absence of contamination of plagioclase analyses by silicate glass (that could be present as melt inclusions in grains or as melt pockets in micro-cracks underneath the surface of exposed plagioclase grains). The bands in Fig. 2 of the main manuscript are interpreted as absorption of structural O-H bond vibrations in plagioclase as opposed to vibrations in contaminant glass for two reasons. First, the OH absorbance measured at a single location in plagioclase grains changes systematically with the rotation of the infrared polariser relatively to the grain during FTIR measurements (Fig. S-1a,c,e). This is inconsistent with the sampling of amorphous glass contamination. In contrast, the OH absorbance in silicate glasses in our experiments remains constant with the rotation of the polariser (Fig. S-1b,d,f). This suggests that the broad band in plagioclase is not caused by contamination. Second, progressive thinning of the samples by repolishing, followed by re-analyses of the thinned samples, indicates that the OH absorbance in plagioclase and glass from our samples is always in linear proportion to sample thickness (Fig. S-2). This demonstrates that the plagioclase spectra are not affected by infrared absorption signals from heterogeneously distributed glass in the light path, nor can they represent combinations of spectra from multiple grains covering each other in the light path through the sample. The similarity between our spectra and previously published work (Johnson and Rossman, 2013; Yang *et al.*, 2015; Liu *et al.*, 2018), combined with the systematic variations in spectra taken at different polarisation angles and sample thicknesses, indicates that our plagioclase data are not affected by glass contamination.

In addition, the water partition coefficients reported by Caseres *et al*. (2017) of experiments at oxygen fugacities lower than those in most of our experiments ($D_{water}^{plag\text{-}melt}$ = 0.018–0.023 at the IW buffer) overlap with our results. The latter study used secondary ion mass spectrometry (SIMS), a time-resolved technique that excels at detecting inhomogeneities, to measure hydrogen abundances in plagioclase and melt. The excellent agreement between our results and these two literature studies lends further support to our conclusion that our plagioclase FTIR data do not suffer from contamination by glass.

3. Oxygen fugacity calculation

To calculate the oxygen fugacities in our experiments, based on our experimental assemblage with an outer-$Au_{80}Pd_{20}$ and inner graphite lining, we use Equation S-2a for the graphite–COH (C-COH) buffer (Ulmer and Luth, 1991) and Equation S-2b for the iron-wustite (IW) buffer (Frost, 1991) systems for iron metal bearing experiments:

$$\log fO_2 \text{ (C-COH buffer)} = (-22324 + 189\cdot P - 1.41\cdot P^2)/T + 4.62 \qquad \text{Eq. S-2a}$$

$$\log fO_2 \text{ (IW buffer)} = -27.489/T + 6.702 + 0.055\cdot(1000\cdot P - 1)/T \qquad \text{Eq. S-2b}$$

where T is the temperature (K), and P is the pressure (kbar). For the Hamada *et al*. (2013) and Caseres *et al.* (2017) experiments, the log(fO_2) was calculated using Frost (1991) for the NNO, FMQ, and IW systems. The calculated log(fO_2) values are shown in Table 1. Our experimental log(fO_2) values from eight samples at the C-COH buffer range from -10.0 to -10.4, which is ~2 log units above the IW buffer (Table 1), consistent with the absence of iron metal blebs in these experimental charges. The log(fO_2) of the single sample at the IW buffer is approximately -12.4 (Table 1), consistent with the presence of iron metal blebs in this experimental charge. The experiments for run products containing Fe-metal from Caseres *et al.* (2017) were performed at the IW buffer, at log(fO_2) = -12.3. The Hamada *et al.* (2013) experiments cover a range of log(fO_2) between -5.8 and -4.7. The fO_2 in our experiments is therefore ~6±2 log units lower than that in previous work focused on terrestrial compositions (Hamada *et al.*, 2013), and overlaps with experimental data reported by Caseres *et al.* (2017) focusing on lunar crust formation.

Supplementary Tables

Table S-1 Nominal compositions of starting materials.

Experiment	SiO_2	TiO_2	Al_2O_3	FeO	MgO	CaO	Water (H_2O)	Total
Pl1_LBS6H	47.54	1.70	15.25	12.88	10.53	10.98	0.59	99.99
Pl2_LBS7H	47.96	1.88	15.68	12.52	9.53	11.19	0.66	100.01
Pl3_LBS8H_1	47.57	2.45	15.48	13.83	7.50	11.52	0.87	99.99
Pl4_LBS8H_2	47.57	2.45	15.48	13.83	7.50	11.52	0.87	99.99
Pl5_LBS8H_3	47.57	2.45	15.48	13.83	7.50	11.52	0.87	99.99
2018_Pl2_LBS8H	47.57	2.45	15.48	13.83	7.50	11.52	0.87	99.99
2018_Pl3_LBS7H	47.96	1.88	15.68	12.52	9.53	11.19	0.66	100.01
2018_Pl17_LBS8H	47.57	2.45	15.48	13.83	7.50	11.52	0.87	99.99
2018_Pl21_LBS5H	48.60	1.60	14.38	13.07	12.52	10.28	0.53	100.45

Compositions in wt. % oxides.

Table S-2 EMPA data of plagioclase and glass in experimental samples.

Experiment	Results								
	Phase	n	SiO_2	TiO_2	Al_2O_3	FeO	MgO	CaO	Total
Pl1_LBS6H	Plagioclase	7	45.59	0.15	33.31	1.23	0.89	18.73	99.9
			(0.51)	(0.01)	(0.29)	(0.08)	(0.07)	(0.34)	
	Glass	9	48.11	1.75	17.05	11.70	7.70	12.38	98.7
			(0.82)	(0.04)	(0.19)	(0.39)	(0.16)	(0.17)	
Pl2_LBS7H	Plagioclase	6	44.77	0.07	34.08	0.89	0.43	19.63	99.9
			(0.44)	(0.01)	(0.32)	(0.07)	(0.03)	(0.37)	
	Glass	10	47.35	1.82	17.54	11.96	7.48	13.24	99.4
			(0.61)	(0.03)	(0.22)	(0.41)	(0.37)	(0.11)	
Pl3_LBS8H_1	Plagioclase	5	46.07	0.08	33.38	0.81	0.46	19.04	99.8
			(0.34)	(0.02)	(0.31)	(0.23)	(0.05)	(0.65)	
	Glass	10	49.03	3.67	14.90	13.96	5.58	12.28	99.4
			(0.75)	(0.05)	(0.17)	(0.35)	(0.18)	(0.31)	
Pl4_LBS8H_2	Plagioclase	5	46.51	0.01	33.27	0.70	0.49	18.89	99.9
			(0.49)	(0.01)	(0.65)	(0.16)	(0.06)	(0.44)	
	Glass	10	49.45	3.19	15.23	13.49	5.52	12.40	99.3
			(0.73)	(0.05)	(0.26)	(0.17)	(0.26)	(0.21)	
Pl5_LBS8H_3	Plagioclase	8	46.11	0.03	33.46	0.66	0.41	18.89	99.6
			(0.22)	(0.01)	(0.36)	(0.09)	(0.02)	(0.12)	
	Glass	10	48.99	3.23	15.02	13.75	5.74	12.71	99.4
			(0.46)	(0.04)	(0.13)	(0.48)	(0.33)	(0.22)	

2018_Pl2_LBS8H	Plagioclase	5	45.96	0.01	33.91	0.58	0.59	18.86	99.9
			(0.33)	(0.01)	(0.35)	(0.06)	(0.03)	(0.32)	
	Glass	6	49.25	3.08	15.43	13.29	5.73	12.88	99.7
			(0.51)	(0.03)	(0.24)	(0.38)	(0.34)	(0.10)	
2018_Pl3_LBS7H	Plagioclase	6	44.79	0.11	34.42	0.73	0.55	19.40	100.0
			(0.38)	(0.02)	(0.41)	(0.21)	(0.05)	(0.35)	
	Glass	7	49.35	4.24	13.25	14.87	6.68	11.42	99.8
			(0.55)	(0.05)	(0.13)	(0.30)	(0.14)	(0.29)	
2018_Pl17_LBS8H	Plagioclase	7	45.89	0.02	33.81	0.56	0.48	18.79	99.6
			(0.42)	(0.01)	(0.26)	(0.07)	(0.02)	(0.19)	
	Glass	9	48.25	3.70	15.10	13.09	5.77	12.72	98.6
			(0.42)	(0.03)	(0.23)	(0.44)	(0.31)	(0.20)	
2018_Pl21_LBS5H	Plagioclase	7	45.90	0.08	33.39	0.89	0.70	18.97	99.9
			(0.59)	(0.01)	(0.55)	(0.17)	(0.06)	(0.42)	
	Glass	8	48.79	2.05	14.79	13.29	9.92	11.04	99.9
			(0.53)	(0.08)	(0.21)	(0.15)	(0.16)	(0.25)	

n, number of analyses; Compositions from EMPA in wt. % oxides with 1σ s.d. in parentheses.

Supplementary Figures

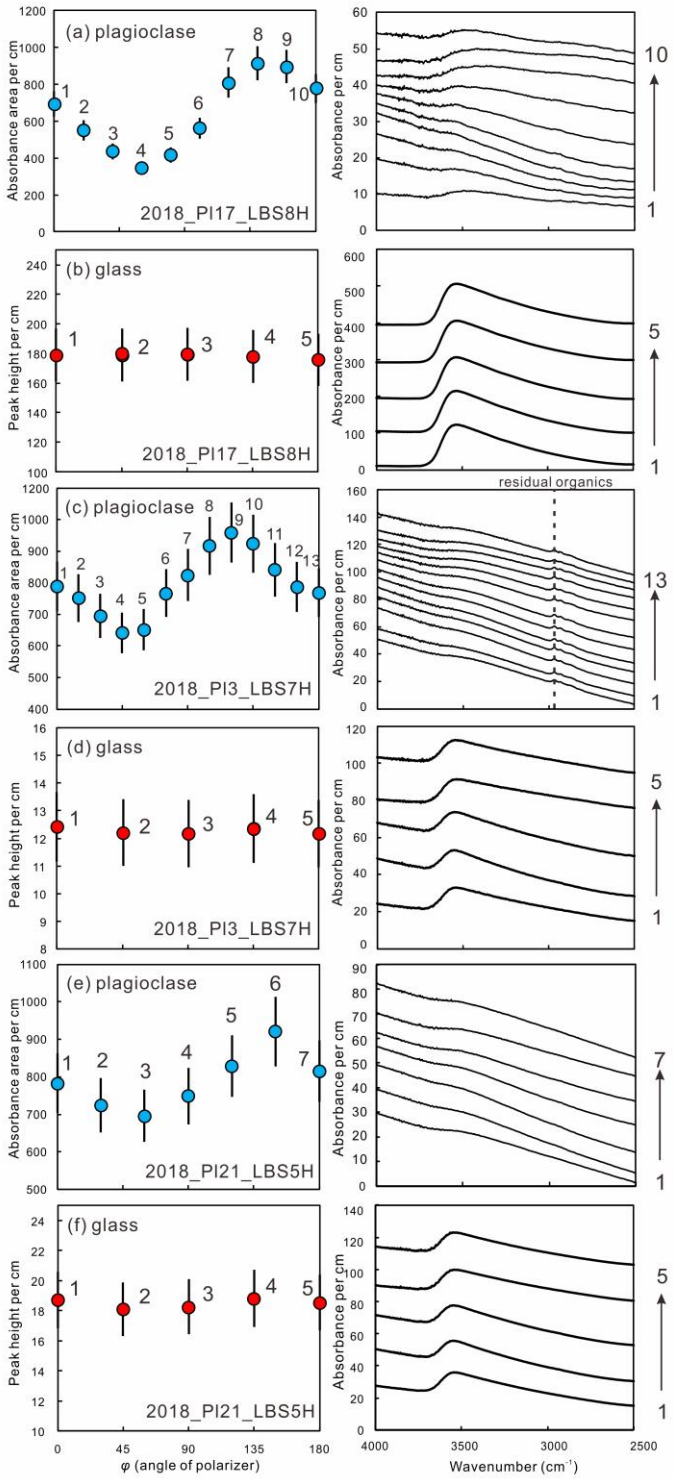

Figure S-1 Systematic variation in OH absorbance (area) of plagioclase **(a, c, e)** and constant OH absorbance (peak height) in glass **(b, d, f)** normalised to sample thickness of 1 cm with the angle of rotation of the infrared polariser, shown together with corresponding raw FTIR spectra**.** No grain was oriented relative to any major axis and the grain orientation was fixed during each series of measurements. FTIR measurements were conducted at a single location on each grain of plagioclase or glass by rotating the polariser relative to the grain orientation. Background measurements were taken in between each of the individual sample measurements. Filled circles show the absorbance calculated as the area beneath the O–H bands (~3600 to ~3000 cm^{-1}) for plagioclase and the absorbance expressed as the OH peak height for glass. Error bars represent ±10 % of the calculated absorbance. The narrow peaks (3000 to 2800 cm^{-1}) most probably come from residual organics on the grain surface during sample preparation.

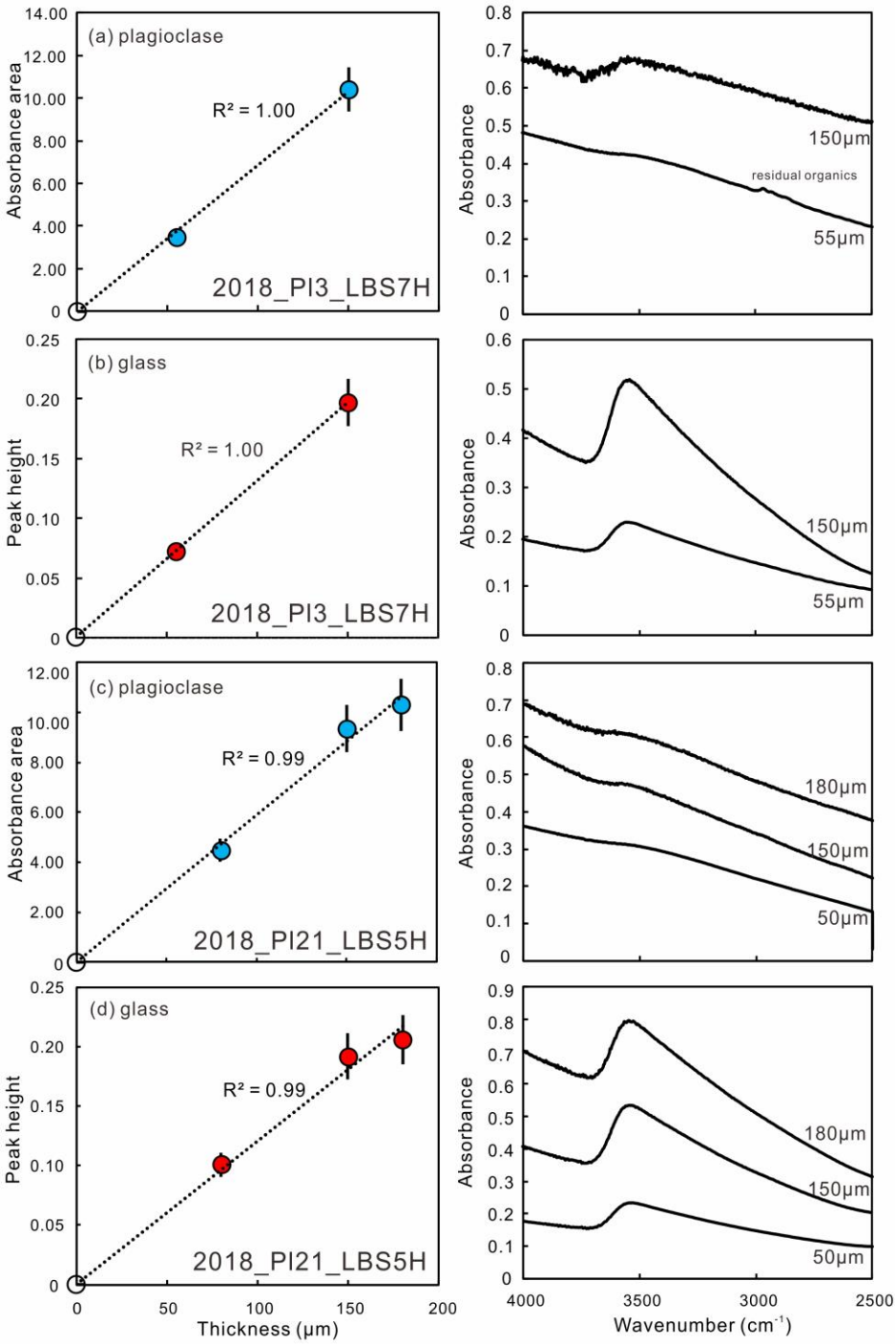

Figure S-2 Linear correlation between OH absorbance area in plagioclase **(a, c)** / peak height in glass **(b, d)** and grain thickness, with corresponding FTIR spectra**.** FTIR measurements were conducted at a single location on each grain / glass spot with the same orientation of the polarizer but different sample thickness. Error bars represent ±10 % of the absorbance.

Supplementary Information References

Caseres, J.R., Mosenfelder, J.L., Hirschmann, M.M. (2017) Partitioning of hydrogen and fluorine between feldspar and melt under the conditions of lunar crust formation. *Abstracts of the Lunar and Planetary Science Conference* 48, 2303.

Frost, B.R. (1991) Introduction to oxygen fugacity and its petrologic importance. *Reviews in Mineralogy and Geochemistry* 25, 1–9.

Hamada, M., Ushioda, M., Fujii, T., Takahashi, E. (2013) Hydrogen concentration in plagioclase as a hygrometer of arc basaltic melts: Approaches from melt inclusion analyses and hydrous melting experiments. *Earth and Planetary Science Letters* 365, 253–262.

Johnson, E.A., Rossman, G.R. (2013) The diffusion behavior of hydrogen in plagioclase feldspar at 800-1000°C: Implications for re-equilibration of OH in volcanic phenocrysts. *American Mineralogist* 98, 1779–1787.

Kovács, I., Hermann, J., O'Neill, H.S.C., Gerald, J.F., Sambridge, M., Horvath, G. (2008) Quantitative absorbance spectroscopy with unpolarized light: Part II. Experimental evaluation and development of a protocol for quantitative analysis of mineral IR spectra. *American Mineralogist* 93, 765–778.

Liu, W.D., Yang, Y., Zhu, K.Y., Xia, Q.K. (2018) Temperature dependences of hydrous species in feldspars. *Physics and Chemistry of Minerals* 45, 609–620.

Sambridge, M., Gerald, J.F., Kovács, I., O'Neill, H.S.C. (2008) Quantitative absorbance spectroscopy with unpolarized light: Part I. Physical and mathematical development. *American Mineralogist* 93, 751–764.

Ulmer, P., Luth, R.W. (1991) The graphite-COH fluid equilibrium in P, T, fO_2 space: An experimental determination to 30 kbar and 1600 ºC. *Contributions to Mineralogy and Petrology* 106, 265–272.

Van Kan Parker, M., Mason, P.R.D., van Westrenen, W. (2011) Experimental study of trace element partitioning between lunar orthopyroxene and anhydrous silicate melt: Effects of lithium and iron. *Chemical Geology* 285, 1–14.

Watson, E.B., Wark, D.A., Price, J.D., van Orman, J. (2002) Mapping the thermal structure of solid-media pressure assemblies. *Contributions to Mineralogy and Petrology* 142, 640–652.

Yamashita, S., Kitamura, T., Kusakabe, M. (1997) Infrared spectroscopy of hydrous glasses of arc magma compositions. *Geochemical Journal* 31, 169–174.

Yang, X., Keppler, H., Li, Y. (2016) Molecular hydrogen in mantle minerals. *Geochemical Perspectives Letters* 2, 160–168.

Yang, Y., Xia, Q.K., Zhang, P.P. (2015) Evolutions of OH groups in diopside and feldspars with temperature. *European Journal of Mineralogy* 27, 185–192.